Parallel Adaptive Mesh Refinment Scheme with Presumed Conditional Moment and FPI Tabulated Chemistry for Turbulent Non-Premixed Combustion

Pradeep K. Jha* and Clinton P. T. Groth†

University of Toronto Institute for Aerospace Studies

4925 Dufferin Street, Toronto, Ontario, Canada, M3H5T6

A parallel, Adaptive Mesh Refinement (AMR), finite-volume scheme is combined with a Presumed Conditional Moment (PCM) and Flame Prolongation of ILDM (FPI) tabulated chemistry approach for solution of the Favre-Averaged Navier-Stokes (FANS) equations governing two-dimensional turbulent non-premixed reactive flows of compressible mixtures. The FPI method is an effective and computationally efficient approach for incorporating the effects of the detailed-chemistry on the local flow field for adiabatic laminar flows using two independent scalars: the mixture fraction and progress variable. The effects of turbulence on the mean chemistry is incorporated using a PCM approach based on β probability density functions which depend on the two scalars and their variances. A two-equation k-ω turbulence model is used for modelling the effects of the unresolved turbulence on the mean flow field. The governing partial-differential equations are solved using a fully-coupled finite-volume formulation on body-fitted, multi-block, quadrilateral mesh. Two different approaches for coupling the PCM-FPI approach with the parallel AMR finite-volume solution method are considered. The PCM-FPI results are compared to results obtained using a simplified Eddy Dissipation Model (EDM), as well as to experimental data, for both reacting and non-reacting flows associated with a bluff-body burner configuration. A full description of the proposed numerical solution scheme for turbulent non-premixed flames is provided along with an evaluation and demonstration of its computational performance and predictive capabilities.

Nomenclature

δ_{ij}	Kronecker delta function
$\dot{\omega}_i$	mass reaction rate of species i produced by the chemical reactions
κ	von Kármán constant = 0.41
$\mathcal{D}_k$	diffusion coefficient for $k = (\mu + \sigma^* \mu_t)$
μ	molecular viscosity depending on fluid properties
ω_{Y_c}	reaction rate of Y_c (sum of the reaction rates of all the species defining Y_c)
$\overline{w}$	time-averaged value of quantity w
ρ	mixture density
θ	azimuthal coordinate of the axisymmetric frame
$\vec{\mathcal{J}}^i$	molecular diffusivity of the species i relative to the main species
$\vec{\vec{\lambda}}$	Reynolds stress tensor
$\vec{\vec{\tau}}$	molecular stress tensor
$\vec{g}$	body force vector
$\vec{q}$	molecular heat flux vector
$\vec{u}$	velocity vector

*Ph.D. Candidate, jhapk@utias.utoronto.ca.

†Professor, groth@utias.utoronto.ca, Senior Member AIAA.

$\vec{\mathcal{J}_t}^{\,i}$	turbulent diffusive fluxes for species i
$\vec{q_t}$	turbulent heat flux vector
ζ	mixture thermal conductivity
c	progress variable $= Y_c(\phi, x)/{Y_c}^{\mathrm{EQ}}(\phi)$
C_f	closure coefficient for f_v transport equation = 1.0
C_p	gas specific heat at constant pressure
C_{mag}	proportionality constant for EDM = 4.0
C_{Y_c}	closure coefficient for Y_{cv} transport equation = 1.0
D_f	diffusion coefficient of $f = \zeta/\rho/C_p$
D_t	turbulent diffusion coefficient $= \mu_t/Sc_t$
D_{Y_c}	diffusion coefficient of $Y_c = \mu/\rho/Sc_{Y_c}$
E	specific total energy $(u_i u_i/2 + h - p/\rho + k)$
h	internal energy $\sum_{k=1}^{N} Y_k h_k$
h_i	absolute internal enthalpy for species i
m	total mass of gas in the volume
m_i	mass of species i present in the given volume
N	total number of species
p	pressure, $p = \sum_{k=1}^{N} \rho Y_k R_k T$
r	radial coordinate of the axisymmetric frame
R_i	gas constant of species i
Sc_i	Schmidt number of species i
Sc_t	turbulent Schmidt number = 1.0
Sc_{Y_c}	Schmidt number of Y_c = 1.0
st	mass stoichiometric ratio of the fuel-oxidizer
T	mixture temperature
u_τ	friction velocity $= \sqrt{\tau_w/\rho}$
w^*	sample space variable for variable w
w_v	variance of quantity w
x	spatial coordinate in the direction normal to the flame front
y	normal distance from the wall
y^+	dimensionless distance from the wall $= u_\tau y/\nu$
Y_F	mass fraction of the fuel
Y_i	mass fraction of species $i = m_i/m$
Y_O	mass fraction of the oxidizer
z	axial coordinate of the axisymmetric frame
τ_w	wall shear stress
${Y_c}^{\mathrm{EQ}}$	value of Y_c in the burnt state (or equilibrium)
f	mixture fraction
ϕ	equivalence ratio
Y_c	progress of reaction
Da	Damköhler number

I. Introduction

Turbulent non-premixed or diffusion flames are very common in many combustion devices such as gas turbine engines and industrial and domestic burners. Understanding the complex physical and chemical processes associated with these flames by numerical techniques has been a central objective of the combustion community for many years.[1] A major challenge in the numerical modelling of turbulent flames is to account for the, in many cases, strong interaction between the turbulence and finite-rate chemistry because of the intense non-linear behaviour of both these phenomena.[2] Also, the length and time scales of the turbulence and chemistry can vary over a very wide range of magnitude in comparison to the characteristic scales of the mean flow.[3] The occurrence of this wide range of scales severely limits the application of direct numerical

simulation (DNS) to extremely simplified synthetic flow problems for turbulent flames and places significant importance on mathematical modelling and approximate techniques.

Understanding detailed chemistry is important for predicting minor intermediate species and pollutants and in order to address problems associated with of autoignition, flame stabilization and recirculating products. The most accurate techniques rely on complex chemistry models. This involves choosing a detailed kinetics scheme and solving a balance equation for the mass fraction of each species involved in the chemical mechanism which can get extremely demanding on the available computational resources. Some simplifying chemistry models have been proposed for turbulent chemistry[4–6] which give a fair indication of the major species concentrations in steady-state flames. However, these methods significantly reduce the number of species involved and hence the number of reactions, and so can only be applied to a limited range of reactive flow problems.[5] The difficulties associated with extending the simplified chemistry models to more complex chemistry[7,8] have pushed to the forefront the need for alternative schemes for modelling detailed chemistry that do not significantly tax available computational resources.

Various techniques have been proposed to reduce combustion chemistry to make it compatible with the numerical solution of practical combustion problems.[3,9–11] Tabulated chemistry approaches, based on the assumption that local flow chemistry is independent of the surrounding flow, are interesting and promising approaches for dealing with complex turbulent flames. A variety of these tabulation methods have been proposed in the past. Peters[9] suggested the use of detailed chemistry solutions of one-dimensional counter-flow flames over varying strain rates for more complex diffusion flame problems. The Intrinsic Low Dimensional Manifold (ILDM) approach, proposed by Mass and Pope,[3] is based on the analysis of the eigenstructure of the source Jacobian to identify slow chemical processes. A pre-computed look-up tables of variables associated with these slow processes is then used during the simulations for evaluating chemical kinetics. Premixed flamelets have been used to tabulate chemistry in turbulent combustion modelling for both premixed and non-premixed flames.[12,13] The Flame Prolongation of ILDM (FPI)[14,15] and Flame Generate Manifold (FGM)[16] are two recently proposed approaches based on tabulation of premixed flamelets. In these methods, the laminar chemical flame structure is stored in a look-up table as a function of only a few independent scalars. Hence, one is only required to solve a rather small set of balance equations for the independent scalars to obtain a rather good representation of the entire flame structure.

An important concern is to incorporate the effects of unresolved turbulence on the reactive flow solutions. Bradley *et al.*[12,17] have shown that probability density functions (PDF) can be used with known laminar flamelet solutions to account for turbulence, and this model has been used in conjunction with Reynolds-averaged Navier-Stokes (RANS) models. A number of studies have validated the use of PDFs for turbulent reacting flows.[18–20] More recently, Vervisch *et al.*,[21] Domingo *et al.*[22,23] and others have adopted a presumed PDF approach, leading to presumed conditional moment (PCM) modelling, in conjunction with the FPI approach for dealing with turbulent chemistry. In this approach, the presumed PDFs for some scalars are used to derive the mean reaction rates and species concentrations. The PCM approach was initially developed for dealing with turbulent premixed flames[15,22,24] and later extended for partially-premixed and diffusion flames.[21,25] These methods have also been extended for performing with Large Eddy Simulation (LES) of turbulent flames[26,27] and have been applied to different combustion regimes.[28,29]

While the potential of LES methods for turbulent reactive flows has certainly been demonstrated, RANS-based approaches are still used in the majority of practical engineering computations and will therefore be the focus here. In the present study, the PCM-FPI approach has been implemented within a block-based, parallel, adaptive-mesh-refinement (AMR), finite-volume scheme for the solution of the Favre-Averaged Navier-Stokes (FANS) equations governing two-dimensional turbulent non-premixed reactive flows of compressible mixtures on body-fitted, multi-block, quadrilateral mesh. This study can be regarded as an extension of the previous parallel solution method development of Northrup and Groth,[30] Gao and Groth[7,31] and Gao *et al.*[32] for turbulent combusting flows to accurately and efficiently account for detailed chemistry. The PCM-FPI approach and the k-ω turbulence model are used to model the effects of the unresolved turbulence, turbulence-chemistry interaction, and provide the necessary simplification for treating the chemical kinetics. Two different approaches for coupling the PCM-FPI approach with the parallel AMR finite-volume solution method are considered. The numerical results of the PCM-FPI approach are compared to results obtained using a simplified Eddy Dissipation Model (EDM), as well as to experimental data, for both reacting and non-reacting flows associated with a bluff-body burner configuration. A full discussion of the proposed solution technique is provide herein along with a demonstration of the computational performance and predictive capabilities of the proposed solution method.

II. Chemical Kinetics for Turbulent Flows

II.A. Presumed Conditional Moment (PCM)

PCM methods are stochastic-based approaches where the reactive and diffusive properties of the flame are described using a joint PDF, P. If the joint PDF of some set of independent variables, $w_1, \ldots, w_N$, is known, the mean value of any quantity, $\varphi = \varphi(w_1, \ldots, w_N)$, can be expressed using the expression

$$\widetilde{\varphi}(x,t) = \int_{w_1} \cdots \int_{w_N} \varphi(w_1^*, \cdots, w_N^*) P(w_1^*, \cdots, w_N^*; x, t) dw_1^* \cdots dw_N^* \tag{1}$$

where $\widetilde{\varphi}$ is the time-averaged value of quantity φ and w^* is the sample space variable for variable w.

In the FPI approach, all thermochemical quantities, φ, are expressed as a function of two variables, the mixture fraction, f, and the progress variable, c, such that

$$\varphi^{\mathrm{FPI}} = \varphi(f, c) \tag{2}$$

where $c = Y_c(\phi, x)/Y_c^{\mathrm{EQ}}(\phi)$, Y_c is the progress of reaction variable, ${Y_c}^{\mathrm{EQ}}$ is the value of Y_c in the burnt state, ϕ is the equivalence ratio, and x is the direction normal to the flame front of the one-dimensional laminar premixed flame. Hence, by simplifying Equation (1), the mean value for FPI tabulated quantities can be expressed as

$$\widetilde{\varphi}(x,t) = \int_{f^*} \int_{c*} \varphi^{\mathrm{FPI}}(f^*, c^*) P(f^*, c^*) dc^* df^* \tag{3}$$

The joint PDF of f and c, given by Equation (3), can be decomposed using the conditional PDF for c for a given value of f^*, $P(c^*|f^*)$, using the relation

$$P(f^*, c^*) = P(c^*|f^*) P(f^*) \tag{4}$$

However, DNS results[21,22] have shown that it is appropriate to treat the mixture fraction and progress variable as statistically independent variables, i.e., $\widetilde{(c|f^*)} \approx \widetilde{c}$, provided an appropriate choice of progress variable is made. This hypothesis of statistical independence is not strictly exact, but has been found to be a reasonable approximation for appropriate choices of Y_c.[22] For example, the linear combination of CO_2 and CO is a suitable choice for methane-air flames.

Substituting Equation (4) in to Equation (3) and using the fact that f and c are statistically independent, the expression for the mean quantity, $\widetilde{\varphi}$, can be approximated by

$$\widetilde{\varphi}(x,t) = \int_{f^*} \int_{c*} \varphi^{\mathrm{FPI}}(f^*, c^*) P(c^*) P(f^*) dc^* df^* \tag{5}$$

In the present study, the PDFs for both mixture fraction and progress reaction, $P(f^*)$ and $P(c^*)$, are assumed to be β-distributions. In general, β-distributions are defined by their first and second moments, i.e., $\widetilde{f}$, f_v, and $\widetilde{c}$, c_v, respectively, and have the form

$$P(Z^*) = \frac{(Z^*)^{(a-1)}(1-Z^*)^{(b-1)}}{\int_0^1 (Z^+)^{(a-1)}(1-Z^+)^{(b-1)} dZ^+} \tag{6}$$

The two parameters, a and b, defining the β-PDF can be determined in terms of the mean and variance as

$$a = \widetilde{Z}\left(\frac{\widetilde{Z}(1-\widetilde{Z})}{Z_v^2} - 1\right) \quad , \qquad b = a\left(\frac{1}{\widetilde{Z}} - 1\right) \tag{7}$$

From the above, it is evident that the mean value of any quantity φ involves determining the value of the four quantities: $\widetilde{f}$, f_v, $\widetilde{c}$ and c_v. For this, balance equations are solved for the mean and variance of mixture fraction and progress of reaction variable, as discussed in detail in Section III.B. Once $\widetilde{Y_c}$ and Y_{cv} are known, c_v can be expressed as

$$c_v = \frac{Y_{cv}}{\widetilde{{Y_c^{\mathrm{Eq}}}^2}} + \widetilde{Y_c}^2 \left(\frac{1}{\widetilde{{Y_c^{\mathrm{Eq}}}^2}} - \frac{1}{\widetilde{{Y_c^{\mathrm{Eq}}}}^2}\right) \tag{8}$$

For practical purposes, two new quantities S_f and S_c, the segregation factor or unmixedness of f and c, are introduced. These quantities are normalized variances of f and c, respectively, and take on values ranging from zero to unity. They are given by

$$S_c = \frac{c_v}{\widetilde{c}(1-\widetilde{c})} \quad , \qquad S_f = \frac{f_v}{\widetilde{f}(1-\widetilde{f})} \tag{9}$$

In the final look-up table for the mean quantities, every chemical quantity is stored as

$$\overline{\varphi} = \varphi^{\mathrm{PCM}}(\widetilde{f}, S_f, \widetilde{c}, S_c) \tag{10}$$

The extension of the FPI approach to flow conditions lying outside the flammability limits of premixed flames for diffusion flames is discussed in a companion paper by Jha and Groth.[33]

Look-up tables for turbulent diffusion flames can become somewhat large and managing the size of the table is an important issue. In the present study for methane-air reacting flows, the dimensions of the table used were $121 \times 20 \times 121 \times 20$. The table was stored in a binary format and a size of 537 MB. Simulations were also carried out using tables with greater resolution to ensure that the chosen size of the table was not too coarse and did not significantly affect predicted solutions.

II.B. Coupling of Turbulence and Chemistry

Three different numerical approaches are used for dealing with chemical kinetics of the methane-air flames considered in this study. The simplest model is the EDM[4] based on a one-step, five-species, chemical kinetic scheme proposed by Westbrook and Dryer[34] for which the one step mechanism is given by

$$\mathrm{CH_4} + 2\,\mathrm{O_2} \longrightarrow \mathrm{CO_2} + 2\,\mathrm{H_2O}$$

The EDM approach assumes that local combustion in the flow is completely limited by the mixing of the reactants and the oxidizer. The specific dissipation rate of turbulent kinetic energy, ω, provides the time scales associated with the turbulence. The mean reaction rate of the fuel, $\widetilde{\dot{\omega}}_F$, is therefore given by

$$\widetilde{\dot{\omega}}_F = C_{mag}\beta_o^*\omega \, \min(\widetilde{Y}_F, \widetilde{Y}_o/st) \tag{11}$$

where C_{mag} is the proportionality constant for EDM set to 4.0, Y_F and Y_O are the mass fractions of the fuel and the oxidizer, respectively, and st is the mass stoichiometric ratio of the fuel-oxidizer. The reaction rates of all other species involved in the reaction are calculated by using the stoichiometric coefficients of each species in the forward chemical reaction mechanism given above.

The PCM-FPI approach for chemical kinetics as described in the previous section uses look-up tables generated using Cantera,[35] an open-source software package for chemically-reactive flows. The Cantera package uses the Gri-Mech 3.0 chemical kinetic mechanism for methane and air involving 53 species and 325 reactions[36] to perform detailed computations of premixed methane-air laminar flames. Two methods are used here to couple the look-up tables with the finite-volume flow solver in the proposed PCM-FPI approach. In both methods, mass fractions from the detailed chemistry solutions for premixed laminar flames are integrated using a presumed conditional moment and stored in a look-up table. The two methods can be summarized as follows:

- **Method 1 - species PDEs are not solved**: Individual species transport equations are not solved. Instead, local values of $\widetilde{f}$, f_v, $\widetilde{Y_c}$, and Y_{c_v} are used to obtain the species concentrations from the table using multi-linear interpolation.

- **Method 2 - species PDEs are solved**: Domingo *et al.*[23] have shown that for fast chemistry/large values of the Damköhler number, Da, the reaction source terms for species and progress of reaction can be related as

$$\dot{\omega}_i \approx \dot{\omega}_{Y_c}\frac{\partial Y_i}{\partial Y_c} \tag{12}$$

  The local values of mass fractions obtained from the look-up table are used to reconstruct the species chemical reaction rates using Equation (12).[23,37] These reaction rates are used in updating the species transport equations.

For all the flames considered herein, radiation losses are not significant and pressure variations are small and therefore the tabulation has been carried out only for a single value of the pressure. This makes the coupling if the tabulation method with the solution method rather straight forward. However, for more general combustion processes involving non-adiabatic flames with acoustical phenomena and/or significant pressure variation, coupling of the tabulation methods to a compressible-flow solution method would be more involved and a multi-pressure tabulation procedure would be required. Refer to the papers by Galpin *et al.*[38] and Vicquelin *et al.*[39] for discussions of the coupling of tabulated chemistry methods with solution methods in these cases.

III. Governing Equations and Numerical Solution Scheme

III.A. Favre-Averaged Navier-Stokes Equations

In this study, the Favre-Averaged Navier-Stokes equations for a compressible thermally perfect gaseous mixture are used to describe turbulent non-premixed reactive flows. In this formulation, neglecting radiation transport and soot formation, the continuity, momentum and energy equations for a N species mixture can be expressed using tensor notation as[40,41]

$$\frac{\partial \bar{\rho}}{\partial t} + \frac{\partial}{\partial x_i}\left(\bar{\rho}\widetilde{u_i}\right) = 0 \tag{13}$$

$$\frac{\partial}{\partial t}\left(\bar{\rho}\widetilde{u_i}\right) + \frac{\partial}{\partial x_i}\left(\bar{\rho}\widetilde{u_j}\widetilde{u_i}\right) = -\frac{\partial \bar{p}}{\partial x_i} + \frac{\partial}{\partial x_i}\left(\bar{\tau}_{ji} + \bar{\rho}\lambda_{ji}\right) \tag{14}$$

$$\begin{aligned}\frac{\partial}{\partial t}\left[\bar{\rho}\left(\widetilde{e} + \frac{\widetilde{u_i}\widetilde{u_i}}{2} + k\right)\right] + \frac{\partial}{\partial x_j}\left[\bar{\rho}\widetilde{u_j}\left(\widetilde{h} + \frac{\widetilde{u_i}\widetilde{u_i}}{2} + k\right)\right] &= \frac{\partial}{\partial x_j}\left[\left(\frac{\mu}{\mathrm{Pr_L}} + \frac{\mu_t}{\mathrm{Pr_t}}\right)\frac{\partial \widetilde{h}}{\partial x_j} + \left(\mu + \sigma^*\frac{\bar{\rho}k}{\omega}\right)\frac{\partial k}{\partial x_j}\right] \\ &+ \frac{\partial}{\partial x_j}\left[\widetilde{u_i}\left(\bar{\tau}_{ij} + \bar{\rho}\lambda_{ij}\right)\right]\end{aligned} \tag{15}$$

where $\overline{w}$ is the time-averaged value of quantity w, $\widetilde{w}$ is the Favre-averaged value of quantity w, $\vec{x}$ is the position vector, ρ is the mixture density, $\vec{u}$ is the velocity vector, p is the pressure $= \sum_{k=1}^{N} \rho Y_k R_k T$, $Y_k = m_k/m$ is the mass fraction of species k, m_k is the mass of species k present in the given volume, m is the total mass of gas in the volume, $\vec{g}$ is the body force vector, $\bar{\tau}_{ji}$ denotes the viscous stress tensor, λ_{ji} denotes the Reynolds stress tensor, e is the specific total energy, h is the internal energy $\sum_{k=1}^{N} Y_k h_k$, h_k is the absolute internal enthalpy for species k and, k is the turbulent kinetic energy, ω is the specific dissipation rate of the turbulent kinetic energy, $\mathrm{Pr_L}$ is the molecular Prandtl number and, $\mathrm{Pr_t}$ is the turbulent Prandtl number (assumed to be a constant value of 0.9 for this work). The viscous stress tensor is given by the constitutive relation

$$\bar{\tau}_{ij} = \mu\left(\frac{\partial \widetilde{u_i}}{\partial x_j} + \frac{\partial \widetilde{u_j}}{\partial x_i}\right) - \frac{2}{3}\delta_{ij}\frac{\partial \widetilde{u_k}}{\partial x_k} \tag{16}$$

where μ is the molecular viscosity and δ_{ij} is the Kronecker delta function. The Boussinesq approximation is used to relate the Reynolds stress tensor, λ_{ij}, to the mean flow strain-rate tensor using a turbulent eddy viscosity, $\mu_t = \bar{\rho}k/\omega$, and is given by

$$\bar{\rho}\lambda_{ij} = \mu_t\left[\frac{\partial \widetilde{u_i}}{\partial x_j} + \frac{\partial \widetilde{u_j}}{\partial x_i} - \frac{2}{3}\delta_{ij}\frac{\partial \widetilde{u_k}}{\partial x_k}\right] - \frac{2}{3}\delta_{ij}\bar{\rho}k \tag{17}$$

The transport equation describing the time evolution of the mass fraction for the k^{th} species, Y_k, is given by

$$\frac{\partial}{\partial t}\left(\bar{\rho}\widetilde{Y_k}\right) + \frac{\partial}{\partial x_j}\left(\bar{\rho}\widetilde{u_j}\widetilde{Y_k}\right) = -\frac{\partial}{\partial x_j}\left[\left(\mathcal{D}^k + \mathcal{D}_t\right)\frac{\partial \widetilde{Y_k}}{\partial x_j}\right] + \widetilde{\dot{\omega}}_k \tag{18}$$

where $\mathcal{D}^k$ is the molecular diffusivity of species k and, $\mathcal{D}_t = \mu_t/\mathrm{Sc}_t$ is the turbulent diffusivity, and Sc_t is the turbulent Schmidt number, taken to be a constant value of 1.0 here.

The modified two-equation k-ω model of Wilcox[42] is used to model the unresolved turbulent flow quantities. Transport equations are solved for the turbulent kinetic energy, k, and the specific dissipation rate, ω, which are given by

$$\frac{\partial}{\partial t}\left(\bar{\rho}k\right)+\frac{\partial}{\partial x_j}\left(\bar{\rho}\widetilde{u}_j k\right)=\bar{\rho}\lambda_{ij}\frac{\partial\widetilde{u}_i}{\partial x_j}-\beta^*\bar{\rho}k\omega+\frac{\partial}{\partial x_j}\left[\left(\mu+\sigma^*\frac{\bar{\rho}k}{\omega}\right)\frac{\partial k}{\partial x_j}\right] \tag{19}$$

$$\frac{\partial}{\partial t}\left(\bar{\rho}\omega\right)+\frac{\partial}{\partial x_j}\left(\bar{\rho}\widetilde{u}_j\omega\right)=\alpha\frac{\omega}{k}\bar{\rho}\lambda_{ij}\frac{\partial\widetilde{u}_i}{\partial x_j}-\beta\bar{\rho}\omega^2+\frac{\partial}{\partial x_j}\left[\left(\mu+\sigma\frac{\bar{\rho}k}{\omega}\right)\frac{\partial\omega}{\partial x_j}\right] \tag{20}$$

where σ^*, β^*, α, σ, and β are closure coefficients for the two-equation model. Thermodynamic and molecular transport properties of each gaseous species are prescribed using Cantera.[35]

III.B. Additional Balance Equations

For the PCM-FPI approach discussed in Section II.A, balance equations must be solved for $\widetilde{f}$, f_v, $\widetilde{Y}_c$, and Y_{cv}. These transport equations have the following forms:

$$\frac{\partial}{\partial t}\left(\overline{\rho}\widetilde{f}\right)+\frac{\partial}{\partial x_i}\left(\overline{\rho}\widetilde{u}_i\widetilde{f}\right)=-\frac{\partial\tau_f}{\partial x_i}+\frac{\partial}{\partial x_i}\left(\overline{\rho}\mathcal{D}_f\frac{\partial\widetilde{f}}{\partial x_i}\right) \tag{21}$$

$$\frac{\partial}{\partial t}\left(\overline{\rho}f_v\right)+\frac{\partial}{\partial x_i}\left(\overline{\rho}\widetilde{u}_i f_v\right)=\frac{\partial}{\partial x_i}\left(\overline{\rho}\mathcal{D}_f\frac{\partial f_v}{\partial x_i}\right)-\frac{\partial}{\partial x_i}\left(\tau_{f^2}-2f\tau_f\right)+2\overline{\rho}\mathcal{D}_f\frac{\partial f}{\partial x_i}\frac{\partial f}{\partial x_i}-2\tau_f\frac{\partial f}{\partial x_i}-2\overline{\rho}\chi_f \tag{22}$$

$$\frac{\partial}{\partial t}\left(\overline{\rho}\widetilde{Y}_c\right)+\frac{\partial}{\partial x_i}\left(\overline{\rho}\widetilde{u}_i\widetilde{Y}_c\right)=-\frac{\partial}{\partial x_i}\left(\tau_{Y_c}\right)+\frac{\partial}{\partial x_i}\left(\overline{\rho}\mathcal{D}_{Y_c}\frac{\partial\widetilde{Y}_c}{\partial x_i}\right)+\overline{\rho}\widetilde{\dot{\omega}}_{Y_c} \tag{23}$$

$$\begin{aligned}\frac{\partial}{\partial t}\left(\overline{\rho}Y_{cv}\right)+\frac{\partial}{\partial x_i}\left(\overline{\rho}\widetilde{u}_i Y_{cv}\right)=&\frac{\partial}{\partial x_i}\left(\overline{\rho}\mathcal{D}_{Y_c}\frac{\partial\widetilde{Y}_c}{\partial x_i}\right)-\frac{\partial}{\partial x_i}\left(\tau_{Y_c{}^2}-2Y_c\tau_{Y_c}\right)+2\overline{\rho}\mathcal{D}_{Y_c}\frac{\partial\widetilde{Y}_c}{\partial x_i}\frac{\partial\widetilde{Y}_c}{\partial x_i}\\&-2\tau_{Y_c}\frac{\partial\widetilde{Y}_c}{\partial x_i}-2\overline{\rho}\chi_{Y_c}+2\overline{\rho}\left(\widetilde{Y_c\dot{\omega}_{Y_c}}-\widetilde{Y}_c\widetilde{\dot{\omega}}_{Y_c}\right)\end{aligned} \tag{24}$$

where $\mathcal{D}_f=\zeta/\bar{\rho}C_p$ is the diffusion coefficient of $\widetilde{f}$, ζ is the mixture thermal conductivity, C_p is the gas specific heat at constant pressure, $\mathcal{D}_{Y_c}=\mu/\bar{\rho}\mathrm{Sc}_{Y_c}$ is the diffusion coefficient of $\widetilde{Y}_c$, $\widetilde{\dot{\omega}}_{Y_c}$ is the reaction rate of Y_c (sum of the reaction rates of all the species defining Y_c) and Sc_{Y_c} is the Schmidt number for the progress variable which is taken to have a constant value of unity herein.

The source terms appearing in Equations (22) and (24) represent the scalar dissipation rate of mixture fraction, χ_f, and the scalar dissipation rate of progress of reaction variable, χ_{Y_c}, respectively, and are closed using linear relaxation hypothesis as follows:

$$\chi_f=\mathcal{D}_t\frac{\partial\widetilde{f}}{\partial x_i}\frac{\partial\widetilde{f}}{\partial x_i}+C_f\omega f_v,\qquad\chi_{Y_c}=\mathcal{D}_t\frac{\partial\widetilde{Y}_c}{\partial x_i}\frac{\partial\widetilde{Y}_c}{\partial x_i}+C_{Y_c}\omega Y_{cv} \tag{25}$$

where C_f and C_{Y_c} are the closure coefficients for f_v and Y_{cv} transport equations, respectively. These closure coefficients are assumed to have values of unity here. All the unclosed turbulent fluxes are modelled using a gradient transport hypothesis and have the forms

$$\tau_f=-\mathcal{D}_t\frac{\partial\widetilde{f}}{\partial x_i},\quad\left(\tau_{f^2}-2f\tau_f\right)=-\mathcal{D}_t\frac{\partial f_v}{\partial x_i},\quad\tau_{Y_c}=-\mathcal{D}_t\frac{\partial\widetilde{Y}_c}{\partial x_i},\quad\left(\tau_{Y_c{}^2}-2Y_c\tau_{Y_c}\right)=-\mathcal{D}_t\frac{\partial Y_{cv}}{\partial x_i} \tag{26}$$

The source quantities, $\widetilde{Y_c\dot{\omega}_{Y_c}}$ and $\widetilde{\dot{\omega}}_{Y_c}$, that appear in Equation (24), are also tabulated in the look-up table along with the species mass fraction. The values of these quantities are extracted from the table based on the local values of the mixture fraction and progress of reaction variables.

III.C. Conservation Form of Equations

For two-dimensional axisymmetric flows, the preceding equations can be re-expressed in conservation form using vector notation as

$$\frac{\partial\mathbf{U}}{\partial t}+\frac{\partial}{\partial r}\left(\mathbf{F}-\mathbf{F}_v\right)+\frac{\partial}{\partial z}\left(\mathbf{G}-\mathbf{G}_v\right)=\frac{1}{r}(\mathbf{S}_a+\mathbf{S}_{av})+\mathbf{S} \tag{27}$$

where r and z are the radial and axial coordinate of the axisymmetric frame, and $\mathbf{U}$ is the vector of conserved variables given by

$$\mathbf{U} = \left[\begin{array}{c} \overline{\rho},\, \overline{\rho}\widetilde{v}_r,\, \overline{\rho}\widetilde{v}_z,\, \overline{\rho}\widetilde{E},\, \overline{\rho}k,\, \overline{\rho}\omega,\, \overline{\rho}\widetilde{f},\, \overline{\rho}f_v,\, \overline{\rho}\widetilde{Y}_c,\, \overline{\rho}Y_{cv},\, \overline{\rho}\widetilde{Y}_1,\, \ldots,\, \overline{\rho}\widetilde{Y}_n \end{array} \right]^{\mathrm{T}} \tag{28}$$

The inviscid and viscous radial flux vectors, $\mathbf{F}$ and $\mathbf{F}_v$, and the inviscid and viscous axial flux vectors, $\mathbf{G}$ and $\mathbf{G}_v$, are

$$\mathbf{F} = \begin{bmatrix} \overline{\rho}\widetilde{v}_r \\ \overline{\rho}\widetilde{v}_r^2 + \bar{p} \\ \overline{\rho}\widetilde{v}_r\widetilde{v}_z \\ (\overline{\rho}\widetilde{E} + \bar{p})\widetilde{v}_r \\ \overline{\rho}\widetilde{v}_r k \\ \overline{\rho}\widetilde{v}_r \omega \\ \overline{\rho}\widetilde{v}_r \widetilde{f} \\ \overline{\rho}\widetilde{v}_r f_v \\ \overline{\rho}\widetilde{v}_r \widetilde{Y}_c \\ \overline{\rho}\widetilde{v}_r Y_{cv} \\ \overline{\rho}\widetilde{v}_r \widetilde{Y}_1 \\ \vdots \\ \overline{\rho}\widetilde{v}_r \widetilde{Y}_n \end{bmatrix}, \mathbf{F}_v = \begin{bmatrix} 0 \\ \overline{\tau}_{rr} + \lambda_{rr} \\ \overline{\tau}_{rz} + \lambda_{rz} \\ \mathcal{B}_r \\ (\mu + \mu_t\sigma^*)\frac{\partial k}{\partial r} \\ (\mu + \mu_t\sigma)\frac{\partial \omega}{\partial r} \\ \overline{\rho}(D_f + D_t)\frac{\partial \widetilde{f}}{\partial r} \\ \overline{\rho}(D_f + D_t)\frac{\partial f_v}{\partial r} \\ \overline{\rho}(D_{Y_c} + D_t)\frac{\partial \widetilde{Y}_c}{\partial r} \\ \overline{\rho}(D_{Y_c} + D_t)\frac{\partial Y_{cv}}{\partial r} \\ -\mathcal{J}_r^1 - \mathcal{J}_{tr}^1 \\ \vdots \\ -\mathcal{J}_r^n - \mathcal{J}_{tr}^n \end{bmatrix}, \mathbf{G} = \begin{bmatrix} \overline{\rho}\widetilde{v}_z \\ \overline{\rho}\widetilde{v}_z\widetilde{v}_z \\ \overline{\rho}\widetilde{v}_z^2 + \bar{p} \\ (\overline{\rho}\widetilde{E} + \bar{p})\widetilde{v}_z \\ \overline{\rho}\widetilde{v}_z k \\ \overline{\rho}\widetilde{v}_z \omega \\ \overline{\rho}\widetilde{v}_z \widetilde{f} \\ \overline{\rho}\widetilde{v}_z f_v \\ \overline{\rho}\widetilde{v}_z \widetilde{Y}_c \\ \overline{\rho}\widetilde{v}_z Y_{cv} \\ \overline{\rho}\widetilde{v}_z \widetilde{Y}_1 \\ \vdots \\ \overline{\rho}\widetilde{v}_z \widetilde{Y}_n \end{bmatrix}, \mathbf{G}_v = \begin{bmatrix} 0 \\ \overline{\tau}_{zr} + \lambda_{zr} \\ \overline{\tau}_{zz} + \lambda_{zz} \\ \mathcal{B}_z \\ (\mu + \mu_t\sigma^*)\frac{\partial k}{\partial z} \\ (\mu + \mu_t\sigma)\frac{\partial \omega}{\partial z} \\ \overline{\rho}(D_f + D_t)\frac{\partial \widetilde{f}}{\partial z} \\ \overline{\rho}(D_f + D_t)\frac{\partial f_v}{\partial z} \\ \overline{\rho}(D_{Y_c} + D_t)\frac{\partial \widetilde{Y}_c}{\partial z} \\ \overline{\rho}(D_{Y_c} + D_t)\frac{\partial Y_{cv}}{\partial z} \\ -\mathcal{J}_z^1 - \mathcal{J}_{tz}^1 \\ \vdots \\ -\mathcal{J}_z^n - \mathcal{J}_{tz}^n \end{bmatrix} \tag{29}$$

where

$$\mathcal{B}_r = -q_r - q_{tr} + (\mu + \mu_t\sigma^*)\frac{\partial k}{\partial r} + v_r(\overline{\tau}_{rr} + \lambda_{rr}) + v_z(\overline{\tau}_{rz} + \lambda_{rz}) \tag{30}$$

$$\mathcal{B}_z = -q_z - q_{tz} + (\mu + \mu_t\sigma^*)\frac{\partial k}{\partial z} + v_r(\overline{\tau}_{zr} + \lambda_{zr}) + v_z(\overline{\tau}_{zz} + \lambda_{zz}) \tag{31}$$

The source terms, $\mathbf{S}_\phi$ and $\mathbf{S}_{\phi v}$, are the inviscid and viscous source vectors associated with the axisymmetric geometry, respectively. The source vector, $\mathbf{S}$, contains terms related to the finite rate chemistry and source terms in transport equations of f_v, c, and c_v. Using

$$\mathcal{W} = v_r(\overline{\tau}_{rr} + \lambda_{rr}) + v_z(\overline{\tau}_{rz} + \lambda_{rz}) \tag{32}$$

$$\mathcal{P} = \lambda_{rr}\frac{\partial \widetilde{v}_r}{\partial r} + \lambda_{rz}\left(\frac{\partial \widetilde{v}_r}{\partial z} + \frac{\partial \widetilde{v}_z}{\partial r}\right) + \lambda_{zz}\frac{\partial \widetilde{v}_z}{\partial z} + \lambda_{\theta\theta}\frac{\widetilde{v}_r}{r} \tag{33}$$

$$\mathcal{Q} = 2\rho D_t \frac{\partial \widetilde{Y}_c}{\partial x_i}\frac{\partial \widetilde{Y}_c}{\partial x_i} - 2C_{Y_c}\rho\omega Y_{cv} + 2\rho\left(\widetilde{Y_c\dot{\omega}_{Y_c}} - \widetilde{Y}_c\widetilde{\dot{\omega}}_{Y_c}\right) \tag{34}$$

these three source vectors have the following forms:

$$\mathbf{S_a} = \begin{bmatrix} \overline{\rho}\widetilde{v}_r \\ \overline{\rho}\widetilde{v}_r^2 \\ \overline{\rho}\widetilde{v}_r\widetilde{v}_z \\ (\overline{\rho}\widetilde{E} + \bar{p})\widetilde{v}_r \\ \overline{\rho}\widetilde{v}_r k \\ \overline{\rho}\widetilde{v}_r \omega \\ \overline{\rho}\widetilde{v}_r \widetilde{f} \\ \overline{\rho}\widetilde{v}_r f_v \\ \overline{\rho}\widetilde{v}_r \widetilde{Y}_c \\ \overline{\rho}\widetilde{v}_r Y_{cv} \\ \overline{\rho}\widetilde{v}_r \widetilde{Y}_1 \\ \vdots \\ \overline{\rho}\widetilde{v}_r \widetilde{Y}_n \end{bmatrix}, \mathbf{S_{av}} = \begin{bmatrix} 0 \\ (\overline{\tau}_{rr} + \lambda_{rr}) - (\overline{\tau}_{\theta\theta} + \lambda_{\theta\theta}) \\ (\overline{\tau}_{rz} + \lambda_{rz}) \\ -q_r - q_{tr} + (\mu + \mu_t\sigma^*)\frac{\partial k}{\partial x} + \mathcal{W} \\ (\mu + \mu_t\sigma^*)\frac{\partial k}{\partial r} \\ (\mu + \mu_t\sigma)\frac{\partial \omega}{\partial r} \\ \overline{\rho}(D_f + D_t)\frac{\partial \widetilde{f}}{\partial r} \\ \overline{\rho}(D_f + D_t)\frac{\partial f_v}{\partial r} \\ \overline{\rho}(D_{Y_c} + D_t)\frac{\partial \widetilde{Y}_c}{\partial r} \\ \overline{\rho}(D_{Y_c} + D_t)\frac{\partial Y_{cv}}{\partial r} \\ -\mathcal{J}_r^1 - \mathcal{J}_{tr}^1 \\ \vdots \\ -\mathcal{J}_r^n - \mathcal{J}_{tr}^n \end{bmatrix}, \mathbf{S} = \begin{bmatrix} 0 \\ 0 \\ 0 \\ 0 \\ \mathcal{P} - \beta^*\rho k\omega \\ \alpha\frac{\omega}{k}\mathcal{P} - \beta\rho\omega^2 \\ 0 \\ 2\rho D_t\frac{\partial \widetilde{f}}{\partial x_i}\frac{\partial \widetilde{f}}{\partial x_i} - 2C_z\rho\omega f_v \\ \rho\widetilde{\dot{\omega}}_{Y_c} \\ \mathcal{Q} \\ \rho\widetilde{\dot{\omega}}_1 \\ \vdots \\ \rho\widetilde{\dot{\omega}}_n \end{bmatrix} \tag{35}$$

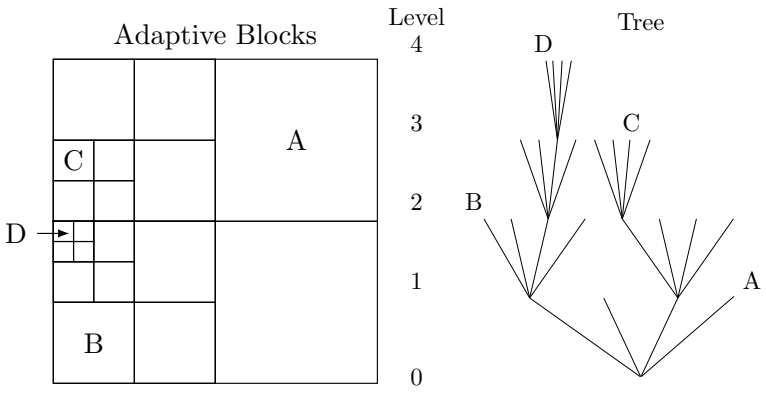

(a) Multi-block refinement (b) Quad-tree structure for 2D AMR

Figure 1: Multi-block quadrilateral AMR mesh showing solution blocks at various levels of refinement and the corresponding quad-tree data structure.

where $\vec{q}$ is the molecular heat flux vector and $\vec{q_t}$ is the turbulent heat flux vector.

III.D. Near Wall Treatment of Turbulence

An automatic wall treatment method, which switches between the low-Reynolds-number formulation and the standard wall function depending on the mesh resolution, is used for near wall treatment of the k-ω turbulence model herein.[31] In the case of low-Reynolds-number formulation, it can be shown that

$$\lim_{y\to 0} \omega = \frac{6\nu}{\beta y^2} \tag{36}$$

where y is the normal distance from the wall. This expression is used to specify the value of ω directly for all values of $y^+ \leq 2.5$, where $y^+ = u_\tau y/\nu$ is the dimensionless distance from the wall, $u_\tau = \sqrt{\tau_w/\rho}$ is the friction velocity, and τ_w is the wall shear stress, provided there are 3-5 computational cells inside $y^+ = 2.5$. In the case of the wall function formulation, the expressions

$$k = \frac{{u_\tau}^2}{\sqrt{\beta_o^*}}, \qquad \omega = \frac{u_\tau}{\sqrt{\beta_o^*}\kappa y} \tag{37}$$

are used to fully specify both k and ω for $y^+ \leq 30 - 250$. The automatic treatment switches between these two methods depending on mesh resolution using a blending function. In this procedure, k and ω are approximated by

$$k = \frac{u_\tau^2}{\beta_o^*}\frac{\min(y^+, 30)}{30}, \qquad \omega = \omega_o\sqrt{1 + \left(\frac{\omega_{wall}}{\omega_o}\right)^2} \tag{38}$$

where $\omega_o = \frac{6\nu}{\beta y^2}$ and $\omega_{wall} = \frac{u_\tau}{\sqrt{\beta_o^*}\kappa y}$. In the turbulent flow simulations discussed below, a relatively coarse mesh is used to start and automatic treatment is used only on the first cell off the wall. After obtaining an approximate solution on the coarse mesh and performing two or three levels of refinement such that there are at least 2-3 cells within the laminar sublayer, the low-Reynolds-number formulation is used for the solution on the finest mesh.

IV. Parallel AMR Finite-Volume Scheme

IV.A. Finite Volume Scheme

A finite volume scheme for body-fitted multi-block quadrilateral mesh is proposed for the solution of the system of partial-differential equations governing two-dimensional axisymmetric turbulent compressible flows for reactive thermally perfect gaseous mixtures given above. In the finite-volume approach, the physical

domain is discretized into finite-sized computational cells (control volumes) and the integral form of the conservation laws are applied to each computational cell. The integral form of the system of governing equations in two-dimensional coordinates can be obtained by applying the divergence theorem to the differential form of the equations and is given by

$$\frac{d}{dt}\int_A \mathbf{U}dA + \oint_l \vec{n}\cdot\vec{\mathbf{F}}\,dl = \int_A \mathbf{S}dA \tag{39}$$

where $\mathbf{U}$ is the vector of conserved variables, $\vec{\mathbf{F}}$ is the flux dyad consisting of both inviscid and viscous flux components, V is the control volume, Ω is the surface area of the control volume and, $\vec{n}$ is the unit outward vector normal to the closed surface.

In the present work, quadrilateral computational cells are considered for the two-dimensional domains of interest. The computational cells are embedded in structured body-fitted blocks making up the multi-block mesh. For each computational cell, the inviscid (hyperbolic) component of the numerical flux at each cell face is then evaluated using limited linear reconstruction[43] and the AUSM$^+$-up approximate Riemann solver proposed by Liou.[44] The viscous (elliptic) component of the numerical flux is evaluated by employing a diamond-path reconstruction procedure as described by.[45] The resulting non-linear ordinary differential equations (ODE) resulting from the spatial discretization are integrated using the explicit multi-stage optimal smoothing scheme of van Leer *et al.*[46] For further details concerning the proposed spatial and temporal discretization schemes, refer to the papers by Northrup and Groth,[30] Charest *et al.*[47] and Gao *et al.*[31]

IV.B. Block-Based Adaptive Mesh Refinement

A flexible block-based AMR scheme is adopted here to limit the number of necessary computational cells by dynamically adapting the mesh to meet solution requirements. Details of the scheme and its implementation in parallel are described by Northrup and Groth,[30] Gao and Groth[7,31] and Gao *et al.*[32] In this approach, block-based domain decomposition is applied to a body-fitted quadrilateral mesh. The grid blocks are organized in a hierarchical quad-tree data structure to facilitate automatic solution-directed mesh adaptation with physics-based criteria. The scheme borrows aspects from previous work by Berger and co-workers,[48–50,50,51] Quirk *et al.*,[52,53] and De Zeeuw *et al.*[54] for Cartesian grids. In the AMR scheme, the equations are first integrated forward in time on an initial structured, multi-block coarse mesh to obtain updated volume-averaged approximate solution quantities. The mesh is then adapted by coarsening or refining the blocks designated by the refinement criteria. A hierarchical tree-like data structure, shown in Figure 1b, is used to retain connectivity between solution blocks and track their refinement history. The blocks requiring refinement are termed "parents" and are divided into eight new blocks called "children". Each child is a new block with the same number of cells as its parent, doubling the mesh resolution in the region. Coarsening flagged blocks is carried out by reversing this process and combining eight children into one single parent.

For the reacting flows of interest here, refinement is based on the gradient of temperature and the refinement criterion employed here is defined by

$$\epsilon \propto |\vec{\nabla}T| \tag{40}$$

The computational mesh is then refined and blocks are added wherever values of ϵ is large. Coarsening is applied in regions where this value is small.

IV.C. Parallel Implementation

To further decrease the overall computational time, integration of the governing equations is performed in parallel. This is carried out by distributing the computational blocks among the available processors and simultaneously computing the solutions for each block on each processor. An even distribution of solution blocks is generally sought on homogeneous architectures while a weighted distribution is permissible for computations performed on heterogeneous systems such as networked workstations or computational grids. To ensure efficient load balancing, blocks are organized using a Morton ordering space filling curve which co-locates nearest neighbors on the same processor.[51] This minimizes the amount of necessary communication and improves the overall parallel efficiency of the implementation. The proposed AMR scheme was implemented using the message passing interface (MPI) library and the C++ programming language.[55]

Ghost cells surround the solution block and overlap cells on neighboring blocks and are used to share solution content through inter-block communication. The conservation properties of the finite-volume discretization are retained across blocks with resolution changes by using the fine-grid interface flux to correct

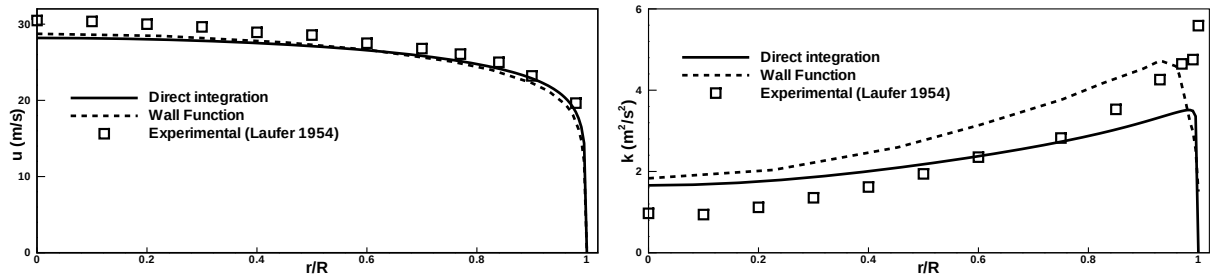

(a) Velocity profile

(b) Turbulent kinetic energy profile

Figure 2: Comparison of predicted solutions with experimental data for fully developed turbulent pipe flow, Re=50 000 .

the flux computed on neighboring coarse blocks.[48,49] Passing of flux corrections and the overlapping cell solution content between processors at each stage of the integration scheme are the main sources of inter-processor communication.

V. Numerical Results and Discussions

V.A. Fully-Developed Turbulent Pipe Flow

As partial validation of the numerical scheme and turbulence modelling, fully-developed turbulent pipe flow case was first considered. Numerical predictions were compared to the experimental data provided by Laufer[56] for a turbulent pipe flow with Reynolds number of 50 000. Solutions for k-ω turbulence model with both direct integration to the wall and standard wall functions are compared to measured mean axial velocity and turbulent kinetic energy in Figures 2. The computations with direct integration are performed using 128 cells in the radial direction with around 13 cells within the laminar sublayer. The first cell from the wall was located at $y^+ \approx 0.04$. The calculations with the wall function formulation were performed using just 32 cells in the radial direction with the first cell at $y^+ \approx 2.54$ and around 6 cells within $y^+ = 250$. Both sets of results provide accurate predictions of the axial velocity profile and expected trends are observed for turbulent kinetic energy. As expected, the present implementation of the k-ω model with direct integration and wall functions are both capable of accurately reproducing the characteristic features of this fully-developed pipe flow.

V.B. Bluff-Body Burner

The Sydney bluff-body burner, which forms part of the experimental database of the International Workshop on Measurement and Computation of Turbulent Non-premixed Flames (TNF),[57] has also been considered in the present work. This burner has been investigated and/or used for verification and validation purposes in several recent studies by Masri *et al.*,[58–61] Dally *et al.*[62,63] and Gao and Groth.[7,8,64] A schematic diagram of the Sydney bluff-body burner configuration is shown in Figure 3.

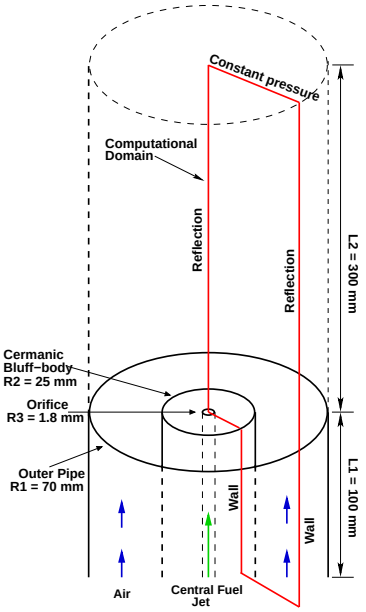

Figure 3: Schematic diagram of the Sydney bluff-body burner. The computational domain and boundary conditions used herein are also shown.

Figure 3 also shows the two-dimensional computational domain used for the numerical simulation of this burner, using the fact that it is an axisymmetric configuration. The bluff-body has a radius $R2 = 25$ mm and length $L1 = 100$ mm and is located co-axially with the air flow inlet. The orifice at the center of the bluff body has a radius $R3 = 1.8$ mm. The outer cylinder for air inflow has a radius of $R1 = 70$ mm. Adiabatic wall boundary conditions are used for the boundaries representing the bluff body. Dirichlet boundary conditions are used for the air inlet and the orifice. The axis of symmetry of the computational

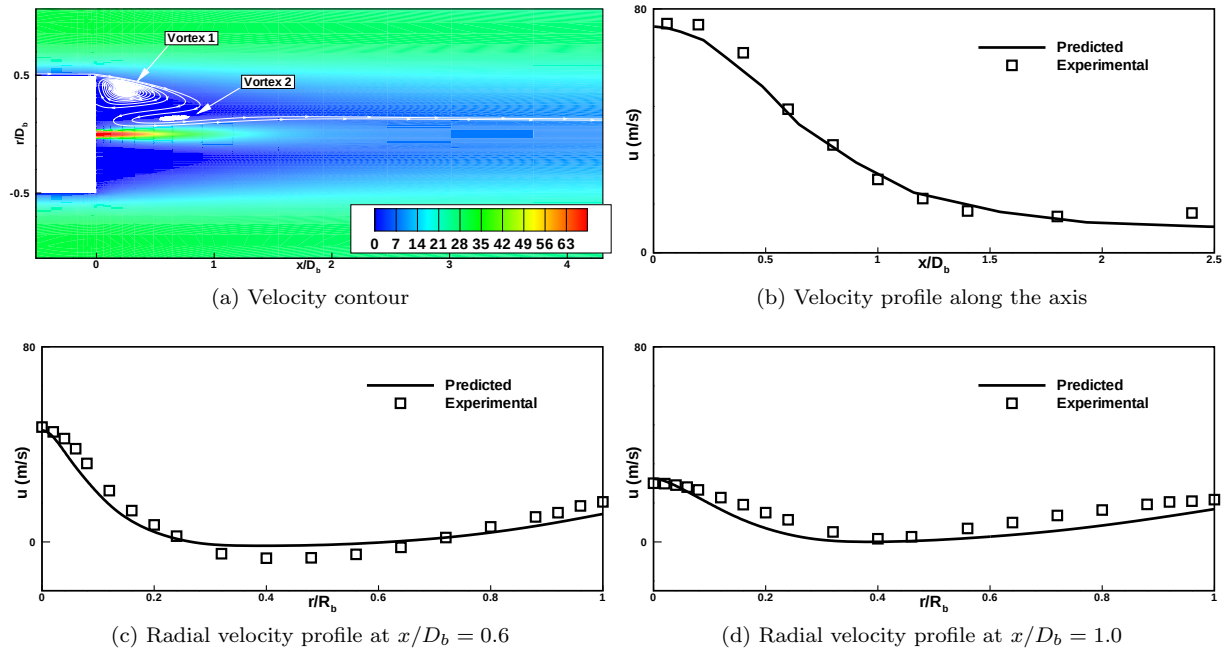

(a) Velocity contour

(b) Velocity profile along the axis

(c) Radial velocity profile at $x/D_b = 0.6$

(d) Radial velocity profile at $x/D_b = 1.0$

Figure 4: Comparison of predicted and measured velocity profiles of mean axial velocity at various locations downstream from the base of the bluff-body burner for non-reacting flow with air jet.

domain is aligned with the centre-line of the bluff-body. A reflection boundary condition is used at the outer boundary. The outlet of the flow domain, at a distance $L2 = 300$ mm from the bluff body, has Neumann-type boundary conditions for all properties except pressure which is held constant.

V.B.1. Non-Reacting Flow

The first bluff-body burner case considered here is a non-reacting flow, where air is injected from both the fuel and the air inlet. Air is injected at the base of the bluff-body at 300 K with a parabolic profile having a mean velocity of 61 m/s. The mean velocity and temperature of the co-flow air are 20 m/s and 300 K respectively. The solution domain is initialized with a uniform solution state corresponding to quiescent air at 300 K. The flow-field calculations were carried out on four adaptively refined grids, each consisting of a number of 8×8 cell blocks: 20 blocks (1280 cells); 38 blocks (3584 cells); 62 blocks (3968 cells); and 101 blocks (6464 cells). The final mesh resolution was such that there were 3-4 cells within the laminar sublayer region close to the wall.

Figure 4a shows the predicted mean axial velocity contours and streamlines and reveals the formation of a double vortex structure in the recirculation zone. The two vortices are important in controlling fuel/oxidizer mixing. The calculations indicate that the recirculation zone extends to $x/D_b \approx 0.8$. This is slightly less than the experimentally observed value of $x/D_b = 1.0$. The agreement between the predictions and experiment is further confirmed by a comparison of the predicted axial (center-line) profile of the mean axial velocity component to the experimental results as depicted in Figure 4b. Also, the comparisons of the predicted radial profiles of the mean axial velocity to the measured data at two locations are shown in Figures 4c and 4d. The results in all these figures clearly indicate that there is reasonably good agreement between the numerical predictions and experimental data. It should also be noted that the predicted results shown here for the non-reacting bluff-body burner configuration are in good agreement with previous numerical predictions of Gao *et al.*[32] (not shown).

V.B.2. Reacting Flow

A reacting flow case for the same bluff-body burner configuration has also been studied, for which a methane gaseous fuel jet was injected at the base of the bluff-body with bulk velocity of 104 m/s at 300 K. The bulk velocity of co-flow air was 30 m/s. The Reynolds and Mach number of the methane jet are Re = 315 000

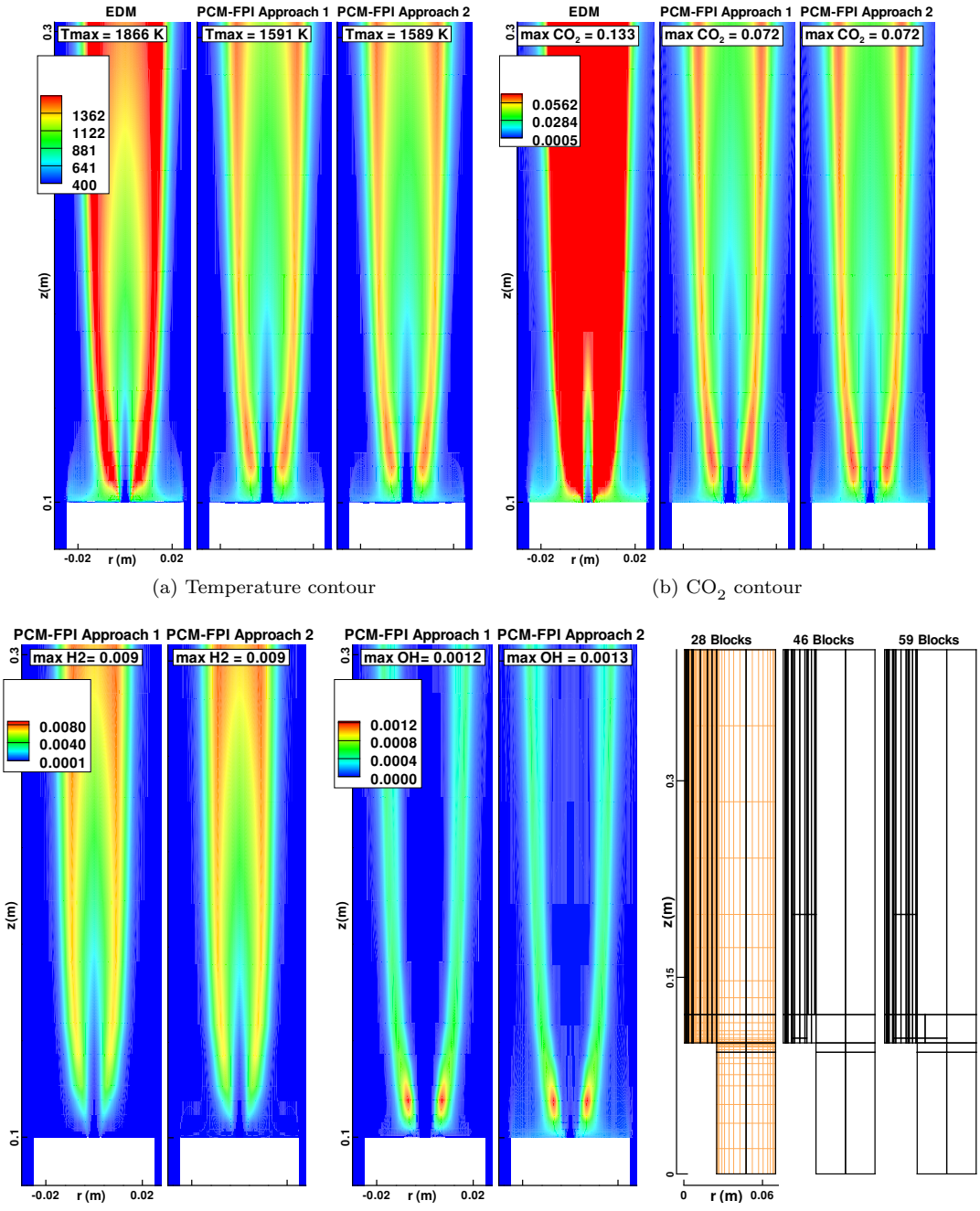

(a) Temperature contour (b) CO_2 contour

(c) H_2 contour (d) OH contour (e) Grid with AMR refinement

Figure 5: The solution contours predicted by different numerical schemes for the Sydney bluff-body burner for a reacting flow with methane jet. The sequence of adaptively refined grids used in the predictions is depicted in Figure 5e.

and Ma = 0.24. The grid used for the the reacting flow is shown in Figure 5e. An initial coarse grid was used containing 28 blocks, each with 16×16 cells, for a total of 7168 cells. After obtaining an approximate solution on this initial mesh, the grid was refined twice using the AMR scheme to arrive at two successively refined grids having the following resolution: 46 blocks (11 776 cells) and 59 blocks (15 104 cells) respectively. The sequence of these adaptively refined mesh is shown in Figure 5e. Inspection of the numerical solutions on these three grids revealed that a near grid converged solution was obtained on the finest mesh and this mesh was used when making comparisons of the predicted results for this case.

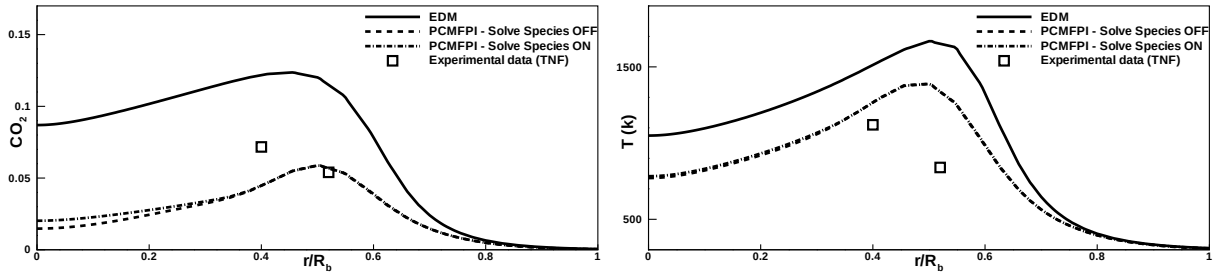

(a) Radial profile of mean mass fraction of CO_2

(b) Radial profile of mean Temperature

Figure 6: Comparison of predicted profiles and measured data at $x/D_b = 1.92$ downstream from the base of the bluff-burner burner for reacting flow with CH_4 jet.

	Experimental	EDM	PCM-FPI (species PDEs = OFF)	PCM-FPI (species PDEs = ON)
(a)	1200 K	1866 K	1591 K	1589 K
(b)	N/A	0.00255 (1)	0.00612 (2.4)	0.00637 (2.5)

Table 1: Performance comparison of different numerical methods for bluff-body burner methane-air turbulent reacting flow: Row (a) Maximum temperature predicted; Row (b): CPU time per iteration - the figures in bracket show the normalized value.

The temperature contours predicted by the proposed solution algorithm with the EDM and the one-step mechanism are compared with the solutions obtained using both the PCM-FPI approaches in Figure 5a for the methane-air bluff-body burner using the 15 104-cell mesh. All three of the schemes predict similar temperature distributions, however the maximum temperature predicted by PCM-FPI schemes are around 300 K less than the value provided by EDM. This is expected as the EDM essentially assumes that any fuel and air that mixes is burnt and does not account for any endothermic reactions, while the PCM-FPI scheme does not assume that the combustion is complete and accounts for endothermic reactions via the tabulated chemistry. Moreover, significant differences can be seen in the distribution of major species contours predicted by both the approaches. The maximum mass fraction of CO_2 predicted by the EDM is almost twice that predicted by the PCM-FPI. This can be attributed to the fact that the EDM reaction mechanism does not involve any pathways or reactions for CO_2 consumption. Also, in the EDM method, much higher concentrations of CO_2 can be found in the central part of the flame compared to the PCM-FPI results, where most of the concentration lies only along the outer surface of the flame.

The predicted temperature and CO_2 mass fraction radial profiles at one location are compared the to the available experimental data in Figure 6. Both figures show that the PCM-FPI results are in much better agreement with the experimental data in comparison to the EDM results. The maximum temperatures predicted by each scheme are shown in Table 1. The temperatures predicted by the PCM-FPI approaches are in better agreement with the experimental results than the EDM results.

It is noted that the temperature is somewhat over-predicted by the proposed parallel AMR scheme for this case. This may be because the effects of radiation and soot formation are not included in the calculations. However, Merci *et al.*[65,66] argue that, since the bluff-body flame is unconfined and very little soot is formed, radiation effects should be relatively small. Some other reasons for the differences may be related to the time averaging of the solution and/or the use of β-distribution for averaging the tabulated quantities. It could be of interest to investigate the dependence of the temperature predictions on the presumed PDF by using other averaging procedures in conjunction with the tabulated chemistry.

The relative cost of each scheme has also been compared in Table 1. As expected, the PCM-FPI schemes are more computationally expensive than the EDM scheme, but the difference is only by a factor of about 2.5. This result is quite significant for it shows that predictions for minor species like H_2, OH, C_2H_2 etc., as shown in Figure 5, can be readily obtained using the tabulation method for less than three times the cost of the EDM. Such predictions are obviously not possible with an EDM approach.

VI. Conclusions

A PCM-FPI tabulation approach for detailed-chemistry has been implemented for turbulent diffusion flames using a FANS-based turbulence model. The two-equation k-ω turbulence model has been used with an automatic-wall-treatment formulation for near-wall-treatment of turbulence quantities. Numerical predictions for fully-developed turbulent pipe flow and non-reacting bluff-body co-flow case were considered. The predicted results for both the non-reacting cases show good agreement with the measured experimental data and provide partial verification of the proposed fully-coupled, parallel, AMR, finite-volume scheme.

Predicted results for a methane-air flame in a bluff-body burner using the PCM-FPI have also been compared to results obtained with a simplified one-step mechanism/EDM approach. As anticipated, significant improvements are observed in the predictions of flame properties using the PCM-FPI approach. The predicted temperature and species profiles using the PCM-FPI approach are in much better agreement with experimental results in comparison to the EDM predictions. Two different approaches for the implementation of the PCM-FPI have been discussed. Both PCM-FPI approaches yield almost identical results for temperature and major species mass fractions. The relative computational costs involved with each numerical schemes is also compared. Even though PCM-FPI schemes tend to be more expensive than the simplified EDM approach, the extra cost is not significantly higher (only slightly more than a factor of two). Comparing the improvement in results for the added computational costs involved, the PCM-FPI approach definitely appears to be a promising method for dealing with a range of turbulent reactive flows. The proposed parallel, AMR, finite-volume scheme has also been shown to be very effective in providing accurate and robust solutions for the reactive flow case. Future work will involve extending the proposed methodology to turbulent non-premixed flame prediction in three-dimensional burner geometries.

Acknowledgments

Computational resources for performing the calculations reported herein were provided by the SciNet High Performance Computing Consortium at the University of Toronto and Compute/Calcul Canada through funding from the Canada Foundation for Innovation (CFI) and the Province of Ontario, Canada.

References

[1]Bilger, R. W., Pope, S. B., Bray, K. N. C., and Driscoll, J. F., "Paradigms in turbulent combustion research," *Proceedings of the Combustion Institute*, Vol. 30, 2005, pp. 21–42.

[2]Veynante, D. and Vervisch, L., "Turbulent Combustion Modeling," *Progress in Energy and Combustion Science*, Vol. 28, 2002, pp. 193–266.

[3]Maas, U. and Pope, S. B., "Simplyfying Chemical Kinetics: Intrinsic Low-Dimensional Manifolds in Composition Space," *Combustion and Flame*, 1992, pp. 239–264.

[4]Magnussen, B. and Hjertager, B., "On mathematical modeling of turbulent combustion with special emphasis on soot formation and combustion," *Sixteenth Symposium (International) on Combustion*, The Combustion Institute, 1976, pp. 719–729.

[5]Sung, C. J., Law, C. K., and Chen, J.-Y., "An Augmented Reduced Mechanism For Methane Oxidation With Comprehensive Global Parametric Validation," *Proceedings of the Combustion Institute*, Vol. 27, 1998, pp. 295–304.

[6]Turns, S. R., editor, *An Introduction to Combustion*, McGraw-Hill, New York, 2000.

[7]Gao, X. and Groth, C. P. T., "Parallel Adaptive Mesh Refinement Scheme for Three-Dimensional Turbulent Non-Premixed Combustion," Paper 2008-1017, AIAA, January 2008.

[8]Gao, X. and Groth, C. P. T., "A Parallel Solution-Adaptive Method for Three-Dimensional Turbulent Non-Premixed Combusting Flows," *J. Comput. Phys.*, Vol. 229, No. 5, 2010, pp. 3250–3275.

[9]Peters, N., "Laminar Diffusion Flamelet Models in Non-Premixed Turbulent Combustion," *Prog. Energy Combustion Sci.*, Vol. 10, 1984, pp. 319–339.

[10]Bilger, R. W., "Conditional Moment Methods for Turbulent Reacting Flows," *Physics of Fluids*, Vol. 5, 1993, pp. 436–444.

[11]Pope, S. B., "Computationally efficient implementation of combustion chemistry using *in situ* adaptive tabulation," *Combustion Theory and Modelling*, Vol. 1, 1997, pp. 41–63.

[12]Bradley, D. and Lau, A. K. C., "The Mathematical Modelling of premixed turbulent combustion," *Pure and Applied Chemistry*, Vol. 62, 1990, pp. 803–814.

[13]Bradley, D., Kwa, L. K., Lau, A. K. C., Missaghi, M., and Chin, S. B., "Laminar flamelet modeling of recirculating premixed methane and propane-air combustion," *Combustion and Flame*, Vol. 71, 1988, pp. 109–122.

[14]Gicquel, O., Darabiha, N., and Thévenin, D., "Laminar premixed hyrogen/air counterflow flame simulations using flame prolongation of ILDM with differential diffusion," *Proceedings of the Combustion Institute*, Vol. 28, 2000, pp. 1901–1908.

[15]Fiorina, B., Gicquel, O., Vervisch, L., Carpentier, S., and Darabiha, N., "Premixed turbulent combustion modeling using tabulated detailed chemistry and PDF," *Proceedings of the Combustion Institute*, Vol. 30, 2005, pp. 867–874.

[16]Oijen, J. A. V. and Goey, L. P. H. D., "Modeling of Premixed Laminar Flames using Flamelet-Generated Manifolds," *Combustion Science and Technology*, Vol. 161, 2000, pp. 113–137.

[17]Bradley, D., Gaskell, P. H., and Gu, X. J., "The Mathematical Modeling of Liftoff and Blowoff of Turbulent Non-premixed Methane Jet Flames At High Strain Rates," *Twenty Seventh Symposium (International) on Combustion*, Vol. 27, 1998, pp.

1199–1206.
[18]Chen, J.-Y. and Dibble, W. K. R. W., "PDF modeling of Turbulent Nonpremixed Methane Jet Flames," *Combustion Science and Technology*, Vol. 64, No. 4, 1989, pp. 315–346.
[19]Norris, A. T. and Pope, S. B., "Modeling of Extinction in Turbulent Diffusion Flames by the Velocity-Dissipation-Composition PDF Method," *Combustion and Flame*, Vol. 100, 1995, pp. 211–220.
[20]Saxena, V. and Pope, S. B., "PDF Simulations of Turbulent Combustion Incorporating Detailed Chemistry," *Combustion and Flame*, Vol. 117, 1999, pp. 340–350.
[21]Vervisch, L., Hauguel, R., Domingo, P., and Rullaud, M., "Three facets of turbulent combustion modelling: DNS of premixed V-flame, LES of lifted nonpremixed flame and RANS of jet-flame," *Journal of Turbulence*, Vol. 4, 2004, pp. 1–36.
[22]Domingo, P., Vervisch, L., and Sandra Payet, R. H., "DNS of a premixed turbulent V flame and LES of a ducted flame using a FSD-PDF subgrid scale closure with FPI-tabulated chemistry," *Combustion and Flame*, 2005, pp. 566–586.
[23]Domingo, P., Vervisch, L., and Veynante, D., "Large-Eddy simulation of a lifted methane jet flame in a vitiated coflow," *Combustion and Flame*, Vol. 152, 2008, pp. 415–432.
[24]Ribert, G., Champion, M., Gicquel, O., Darabiha, N., and Veynante, D., "Modeling nonadiabatic turbulent premixed reactive flows including tabulated chemistry," *Combustion and Flame*, Vol. 141, May 2005, pp. 271–280.
[25]Fiorina, B., Gicquel, O., Vervisch, L., Carpentier, S., and Darabiha, N., "Approximating the chemical structure of partially premixed and diffusion counterflow flames using FPI flamelet tabulation," *Combustion and Flame*, Vol. 140, 2005, pp. 147–160.
[26]F.E.Hernàndez-Pérez, Yuen, F., Groth, C., and Ö.L.Gulder, "LES of a laboratory-scale turbulent premixed Bunsen flame using FSD, PCM-FPI and thickened flame models," accepted in the Proceedings of the Combustion Institute, doi:10.1016/j.proci.2010.06.010., 2010.
[27]Subramanian, V., Domingo, P., and Vervisch, L., "Large eddy simulation of forced ignition of an annular bluff-body burner," *Combustion and Flame*, Vol. 157, 2010, pp. 579–601.
[28]Michel, J.-B., Colin, O., and Veynante, D., "Comparison of Differing Formulations of the PCM Model by their Application to the Simulation of an Auto-igniting H_2/air jet," *Flow Turbulence Combustion*, 2009, pp. 33–60.
[29]Michel, J.-B., Colin, O., Angelberger, C., and Veynante, D., "Using the tabulated diffusion flamelet model ADF-PCM to simulate a lifted methane-air jet flame," *Combustion and Flame*, Vol. 156, 2009, pp. 1318–1331.
[30]Northrup, S. A. and Groth, C. P. T., "Solution of Laminar Diffusion Flames Using a Parallel Adaptive Mesh Refinement Algorithm," Paper 2005–0547, AIAA, January 2005.
[31]Gao, X. and Groth, C. P. T., "Parallel Adaptive Mesh Refinement Scheme for Turbulent Non-Premixed Combusting Flow Prediction," Paper 2006-1448, AIAA, January 2006.
[32]Gao, X., Northrup, S., and Groth, C. P. T., "Parallel solution-adaptive method for two-dimensional non-premixed combusting flows," accepted in the Progress in Computational Fluid Dynamics, 2010.
[33]Jha, P. K. and Groth, C. P. T., "Evaluation of Flame-Prolongation of ILDM and Flamelet Tabulated Chemistry Approaches for Laminar Flames," Submitted for presentation at 49th AIAA Aerospace Sciences Meeting including the New Horizons Forum and Aerospace Exposition at Orlando, Florida, January 2011.
[34]Westbrook, C. K. and Dryer, F. L., "Simplified Reaction Mechanisms for the Oxidation of Hydrocarbon Fuels in Flames," *Combust. Sci. Tech.*, Vol. 27, 1981, pp. 31–43.
[35]Goodwin, D. and Moffat, H. K., "Cantera," http://www.cantera.org.
[36]Smith, G. P., Golden, D. M., Frenklach, M., Moriarty, N. W., Eiteneer, B., Goldenberg, M., Bowman, C. T., Hanson, R. K., Song, S., Gardiner, W. C., Lissianski, V. V., and Qin, Z., "GRI-Mech 3.0," http://www.me.berkeley.edu/gri_mech/.
[37]Galpin, J., Naudin, A., Vervich, L., Christian Angelberger, O. C., and Domingo, P., "Large-eddy simulation of a fuel-lean premixed turbulent swirl-burner," *Combustion and Flame*, Vol. 155, 2008, pp. 247–266.
[38]Galpin, J., *Modélisation LES de la combustion avec une prise en compte des effets de cinétique détaillée et en perspective d'application moteur*, Ph.D. thesis, IFP, Division Techniques d'Applications Énergétiques, September 2007.
[39]Vicquelin, R., Fiorina, B., Payet, S., Darabiha, N., and Gicquel, O., "Coupling tabulated chemistry with compressible CFD solvers," Accepted in the Proceedings of the Combustion Institute, 2011.
[40]Kuo, K., *Principles of Combustion*, John Wiley & Sons, 1986.
[41]Aris, R., *Vectors, Tensors and the Basic Equations of Fluid Mechanics*, Dover Publications, New Jersey, 1989.
[42]Wilcox, D., *Turbulence Modeling for CFD*, DCW Industries, 2002.
[43]Barth, T. J., "Recent Developments in High Order K-Exact Reconstruction on Unstructured Meshes," Paper 93-0668, AIAA, January 1993.
[44]Liou, M.-S., "A Sequel to AUSM, Part II: AUSM$^+$-up for all speeds," *J. Comput. Phys.*, Vol. 214, 2006, pp. 137–170.
[45]Coirier, W. J. and Powell, K. G., "Solution-Adaptive Cartesian Cell Approach for Viscous and Inviscid Flows," *AIAA J.*, Vol. 34, No. 5, May 1996, pp. 938–945.
[46]van Leer, B., Tai, C. H., and Powell, K. G., "Design of Optimally-Smoothing Multi-Stage Schemes for the Euler Equations," Paper 89-1933-CP, AIAA, June 1989.
[47]Charest, M. R., Groth, C. P. T., and Gülder, O. L., "A computational framework for solving laminar reacting flows with soot formation," Submitted to Combustion Theory and Modelling, 2010.
[48]Berger, M. J., "Adaptive Mesh Refinement for Hyperbolic Partial Differential Equations," *J. Comput. Phys.*, Vol. 53, 1984, pp. 484–512.
[49]Berger, M. J. and Colella, P., "Local Adaptive Mesh Refinement for Shock Hydrodynamics," *J. Comput. Phys.*, Vol. 82, 1989, pp. 67–84.
[50]Berger, M. J. and Saltzman, J. S., "AMR on the CM-2," *Appl. Numer. Math.*, Vol. 14, 1994, pp. 239–253.
[51]Aftosmis, M. J., Berger, M. J., and Melton, J. E., "Robust and Efficient Cartesian Mesh Generation for Component-Base Geometry," *AIAA J.*, Vol. 36, No. 6, 1998, pp. 952–960.
[52]Quirk, J. J., *An Adaptive Grid Algorithm for Computational Shock Hydrodynamics*, Ph.D. thesis, Cranfield Institute of Technology, January 1991.
[53]Quirk, J. J. and Hanebutte, U. R., "A Parallel Adaptive Mesh Refinement Algorithm," Report 93-63, ICASE, August 1993.
[54]De Zeeuw, D. and Powell, K. G., "An Adaptively Refined Cartesian Mesh Solver for the Euler Equations," *J. Comput. Phys.*, Vol. 104, 1993, pp. 56–68.
[55]Gropp, W., Lusk, E., and Skjellum, A., *Using MPI*, MIT Press, Cambridge, Massachussets, 1999.
[56]J.Laufer, "The Structure of Turbulence in Fully Developed Pipe Flow," Report 1174, NACA, 1954.

[57] "International Workshop on Measurement and Computation of Turbulent Nonpremixed Flames," http://www.ca.sandia.gov/TNF/.
[58] Masri, A. R., Dibble, R. W., and Barlow, R. S., "The Structure of Turbulent Nonpremixed Flames of Methanol over a Range of Mixing Rates," *Combustion and Flame*, Vol. 89, 1992, pp. 167–185.
[59] Masri, A. R., Dibble, R. W., and Barlow, R. S., "Raman-Rayleigh Measurements in Bluff Body Stabilised Flames of Hydrocarbon Fuels," *Twenty-fourth Symposium (International) on Combustion*, The Combustion Institute, 1992, pp. 317–324.
[60] Masri, A. R., Dally, B. B., and Barlow, R. S., "The Structure of the Recirculation Zone of a Bluff-Body Combustor," *Twenty-fifth Symposium (International) on Combustion*, The Combustion Institute, 1994, pp. 1301–1308.
[61] Masri, A. R., Kelman, J. B., and Dally, B. B., "The Instantaneous Spatial Structure of the Recirculation Zone in Bluff-Body Stabilised Flames," *Proceedings of the Combustion Institute*, The Combustion Institute, 1998, pp. 1031–1038.
[62] Dally, B. B., Fletcher, D. F., and Masri, A. R., "Modelling of Turbulent Flames Stabilised on a Bluff-Body," *Combust. Theory Modelling*, Vol. 2, 1998, pp. 193–219.
[63] Dally, B. B., Masri, A. R., Barlow, R. S., and Fiechtner, G. J., "Instantaneous and Mean Compositional Structure of Bluff-Body Stabilised Nonpremixed Flames," *Combust. Theory Modelling*, Vol. 114, 1998, pp. 119–148.
[64] Gao, X. and Groth, C. P. T., "A Parallel Adaptive Mesh Refinement Algorithm for Predicting Turbulent Non-Premixed Combusting Flows," *Int. J. Comput. Fluid Dyn.*, Vol. 20, No. 5, 2006, pp. 349–357.
[65] Merci, B., *An Unstructured Parallel Algorithm for Large Eddy and Conjugate Heat Transfer Simulations*, Ph.D. thesis, Ghent University, 2000.
[66] Merci, B., Dick, E., Vierendeels, J., Roekaerts, D., and Peeters, T. W. J., "Application of a New Cubic Turbulence Model to Piloted and Bluff-Body Diffusion Flames," *Combust. Flame*, Vol. 126, No. 1-2, 2001, pp. 1533–1556.